Carbohydrate Research 344 (2009) 1197–1204

Contents lists available at ScienceDirect

Carbohydrate Research

journal homepage: www.elsevier.com/locate/carres

Polyelectrolyte nanoparticles based on water-soluble chitosan–poly(L-aspartic acid)–polyethylene glycol for controlled protein release

Shujun Shu, Xinge Zhang *, Dayong Teng, Zhen Wang, Chaoxing Li *

The Key laboratory of Functional Polymer Material of Ministry of Education, Institute of Polymer Chemistry, Nankai University, 94# Weijin Road, Tianjin 300071, PR China

ARTICLE INFO

Article history:
Received 26 November 2008
Received in revised form 12 April 2009
Accepted 16 April 2009
Available online 20 April 2009

Keywords:
Water-soluble chitosan
Poly(L-aspartic acid)
Polyethylene glycol
Polyelectrolyte nanoparticles
Protein drug delivery

ABSTRACT

Water-soluble chitosan (WSC)–poly(L-aspartic acid) (PASP)–polyethylene glycol (PEG) nanoparticles (CPP nanoparticles) were prepared spontaneously under quite mild conditions by polyelectrolyte complexation. These nanoparticles were well dispersed and stable in aqueous solution, and their physicochemical properties were characterized by turbidity, FTIR spectroscopy, dynamic light scattering (DLS), transmission electron microscope (TEM), and zeta potential. PEG was chosen to modify WSC–PASP nanoparticles to make a protein-protective agent. Investigation on the encapsulation efficiency and loading capacity of the bovine serum albumin (BSA)-loaded CPP nanoparticles was also conducted. Encapsulation efficiency was obviously decreased with the increase of initial BSA concentration. Furthermore, its in vitro release characteristics were evaluated at pH 1.2, 2.5, and 7.4. In vitro release showed that these nanoparticles provided an initial burst release, followed by a slowly sustained release for more than 24 h. The BSA released from CPP nanoparticles showed no significant conformational change compared with native BSA, which is superior to the BSA released from nanoparticles without PEG. A cell viability study suggested that the nanoparticles had good biocompatibility. This nanoparticle system was considered promising as an advanced drug delivery system for the peptide and protein drug delivery.

1. Introduction

Significant advances in biotechnology and genetic research have resulted in the discovery of a large number of proteins and peptides that are very effective in disease treatment.[1,2] Routinely, peptides and proteins are administered through the parenteral route, which has poor absorption efficiency in patients. Therefore, a large amount of work has focused on protein delivery by the oral route.[3–5] However, the bioavailability of peptide after oral administration is low due to instability and poor absorption of proteins in the gastrointestinal (GI) tract under most circumstances. One possible way to improve the GI uptake of peptides is to encapsulate them in colloidal nanoparticles that can protect the peptides from being degraded in the GI tract and facilitate their transportation into systemic circulation.[6,7]

Polymeric nanoparticles have been widely investigated as carriers for drug delivery.[7,8] Among them, much attention has been paid to the nanoparticles that are made of synthetic biodegradable polymers such as poly(ε-caprolactone) and polylactide due to their good biocompatibilities.[9,10] However, these nanoparticles are not ideal carriers for hydrophilic protein drugs because of their hydrophobic properties.

Owing to the special capability of a polyelectrolyte complex, many complex phenomena in an organism, such as the transfer of gene information, and the interaction between an antibody and its antigen, are related to these complexes, either directly or indirectly. These interactions could contribute to the simulation of the process in an organism and to the accomplishment of some special functions.[11] In particular, a polyelectrolyte complex is obtained when two polymers carrying opposite charges are mixed and interact via electrostatic interactions.

Chitosan (CS), a weak cationic polysaccharide produced by deacetylation of the natural polymer chitin, has many useful biological properties, such as biocompatibility, biodegradability, and bioactivity. Because of the existence of amine groups, CS is a polycation and is able to form intermolecular complexes with a wide variety of polyanions including hyaluronic acid,[12–14] poly(galacturonic acid),[15] alginate,[16] gelatin,[17] dextran sulfate,[18] and poly(acrylic acid).[19–21] Most commercially available CS has a quite large molecular weight (M_r) and needs to be dissolved in an acetic acid solution at a pH value of approximately 4.0. However, there are potential applications of CS in which a low M_r would be essential. Given a low M_r, the polycationic characteristics of water-soluble chitosan can be used together with a good solubility at a pH value close to physiological ranges. Loading of peptide or protein drugs at physiological pH ranges may prevent their bioactivity from decreasing.[22] WSC can improve the transportation of hydrophilic drugs across the intestinal epithelium, and it is

* Corresponding authors. Tel.: +86 22 2350 1645; fax: +86 22 2350 5598 (C.L.).
E-mail addresses: zhangxinge@nankai.edu.cn (X. Zhang), lcx@nankai.edu.cn (C. Li).

0008-6215/$ - see front matter © 2009 Elsevier Ltd. All rights reserved.
doi:10.1016/j.carres.2009.04.018

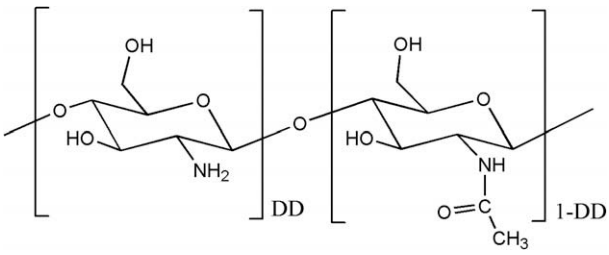

Figure 1. Chemical structure of WSC (DD is the degree of deacetylation).

believed that WSC can increase the permeability of epithelial tissues by disrupting intercellular tight junctions.[23,24] On this basis, water-soluble chitosan, was used to study the preparation of nanoparticles.

PASP is a poly(α-amino acid), which can be classified as a weak synthetic polyelectrolyte. Poly(amino acids) would seem to have considerable advantages over other polymers owing to their protein-like structure. PASP is of potential interest for being used as a biodegradable water-soluble poly(carboxylic acid).

PEG is a nontoxic hydrophilic polymer which is widely used for protein conjugation and protein purification. Segmental flexibility and uncharged chemical composition of PEG help to easily adapt their conformations to fit the surface topology of proteins.[25] PEG is reported to abrogate immunogenicity of proteins while preserving their biological activity, and PEG-conjugated peptides are widely investigated for the applications of drug delivery.[26,27] As these derivatives are uncharged in nature, incorporation of linear PEG chains enhances the mucoadhesive property of the nanoparticle systems by improving mobility and flexibility.[28]

In this study, a novel nanoparticles system, composed of WSC, PEG, and PASP, was prepared by a simple coagulation method. Polyelectrolyte complexes consisting of WSC and PASP may possess merit of both WSC and PASP, and these have a broad range of uses in biomedical applications. However, there are only few reports concerning WSC–PASP–PEG complexes available in the literature.[29]

Based on the reasons mentioned above, the aim of this paper is to develop a new nanoparticulate system, composed of WSC, PASP, and PEG. Physicochemical characteristics of the prepared nanoparticles were characterized by Fourier-transform infrared (FTIR) spectroscopy, dynamic light scattering (DLS), transmission electron microscopy (TEM), and zeta potential. The potential of WSC–PASP–PEG nanoparticles, which are regarded as a carrier system for a model protein, bovine serum albumin (BSA), was also presented.

2. Experimental

2.1. Materials

WSC with an M_r = 6 kDa was purchased from Yuhuan Ocean Biochemical Co., Ltd (Zhejiang, China), and the degree of deacetylation was 0.93 (Fig. 1). Polyethylene glycol (M_r = 4 kDa) was obtained from Tianjin Ke Mi Ou Chemical Co., Ltd. (Tianjin, China). L-Aspartic acid was purchased from Beijing Xing Jing Ke Biotechnology Co., Ltd BSA, with an M_r of 66.7 kDa, was purchased from Beijing Jun Yao Wei Ye Biotechnology Co., Ltd Coomassie brilliant blue G-250 was obtained from Fiuka (Milwaukee, USA). All other reagents were of analytical grade and were used without further purification.

2.2. Preparation of PASP

Poly(succinimide) (PSI) was synthesized by the acid-catalyzed thermal polycondensation of L-aspartic acid as previously reported.[30,31] Upon hydrolysis of PSI in aqueous NaOH, poly(L-aspartic acid) was obtained. This PASP consists of L-aspartic acid repeating units in the α and β forms (Scheme 1). The ratio of α to β form, which was determined by the area ratio in the ^{1}H NMR spectrum, was 26:74, indicating that the β form predominated rather than α form.[30] Viscosity measurements were carried out using an Ubbelohde-type viscometer, with temperature control in the range of 25 ± 0.1 °C, M_v = 23 kDa. The weight-average molecular weights of PASP were measured to be 22.9 kDa by gel-permeation chromatography (Waters 510, USA), M_r = 22.9 kDa, PDI = 1.402.

2.3. Turbidimetric titration measurement

The interactions between PASP and WSC were investigated by turbidimetric titration according to the reported method.[31] A solution of 2 mg/mL PASP and 2 mg/mL WSC was prepared at pH 6.8. Titrant was delivered to each sample with a microburette under gentle stirring, and the pH was monitored by a digital pH meter. Changes in turbidity were monitored at 500 nm by a UV–vis spectrophotometer, and the turbidity was estimated by the absorbance.

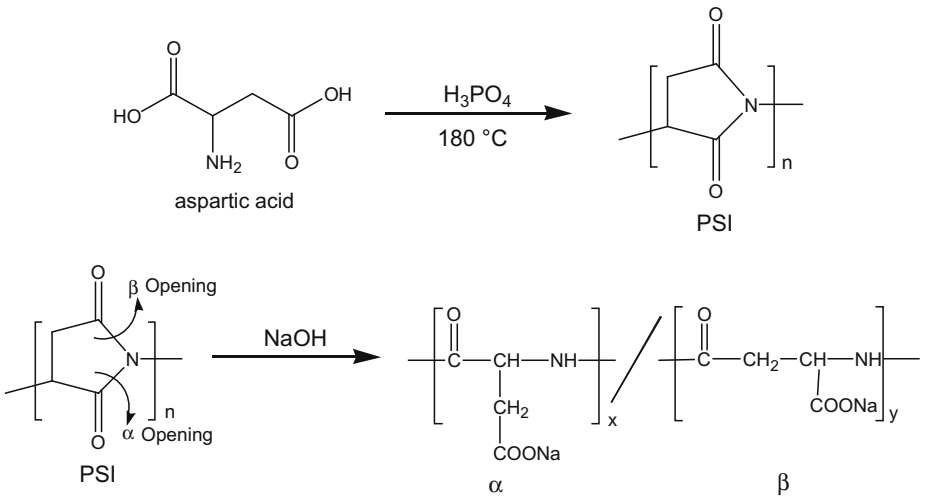

Scheme 1. Preparation of PASP.

2.4. Preparation of WSC–PASP–PEG nanoparticles

CPP nanoparticles were prepared by mixing negatively charged PASP and positively charged WSC and PEG by a dropping method. The procedure is as follows: 200 mg of chitosan was dissolved in 100 mL of deionized water (2 mg/mL, w/v) under magnetic stirring at room temperature without addition of acetic acid and the solution was stirred for 12 h and filtered by filter paper. PASP (200 mg) was dissolved in 100 mL of deionized water, stirred for 12 h, and filtered by the filter paper. Afterwards, the WSC solution was dropped into PASP solution in different molar ratios under magnetic stirring. And then, the resultant opalescent emulsion was stirred for 30 min to allow nanoparticles to form uniform particles. These nanoparticles were isolated by ultracentrifugation at 40,000 rpm for 30 min at 4 °C.

2.5. pH measurement

WSC–PASP–PEG nanoparticles were prepared at pH 6.8, and dilute NH_4OH or dilute HOAc was added to obtain different pH values. The pH value was measured at 20 ± 0.1 °C in a PHS-3TC digital pH meter with an error of 0.01 pH units. A combined glass electrode E-201 was employed, and the pH-meter was calibrated with two buffer solutions supplied by Shanghai Hongbei Reagent Factory.

2.6. Determination of process yield

For the calculation of the nanoparticle production yields, the nanoparticle suspensions were centrifuged at 40,000 rpm for 1 h, and the supernatants were discarded. The tubes containing the sediments were freeze dried for 24 h, and the difference in the theoretical solid weights and the actual freeze-dried nanoparticles weights was determined. The yield of the process was calculated as follows:[32]

$$\text{Process yield } \% = \frac{\text{nanoparticles weight}}{\text{total solids (CS + PASP) weight}} \times 100\%$$

2.7. Evaluation of nanoparticles stabilities

The stabilities of the nanoparticles were investigated in phosphate buffer solution (PBS) at pH 7.4 at room temperature. Aliquots of fresh suspensions of nanoparticles were diluted with the addition of PBS, reaching a concentration 1 mg/mL, and the evolution of the size was assessed by photon correlation spectroscopy for several hours at room temperature.

2.8. Preparation of drug-loaded WSC–PASP–PEG nanoparticles

The drug-loaded nanoparticles were prepared by dropping a mixture of PASP and BSA into WSC–PEG solution. PASP was dissolved in 4 mL of deionized water at a specified concentration (0.1, 0.5, 1.0, 1.5, and 2.0 mg/mL), and 2 mL of BSA (2 mg/mL) was added. Then this solution was dropped into a mixture solution of 4 mL of a specified concentration (0.1, 0.5, 1.0, 1.5, and 2.0 mg/mL) of WSC–PEG solution and 2 mL of deionized water, while sonicating with an ultrasonic sonicator at 160 W.

2.9. Particles size and zeta potential measurement

The size of self-aggregates was measured by a dynamic light scattering method based on the particle size option in Zeta Plus (Brookhaven Instruments Co., Holtsville, New York, He–Ne laser). The scattered intensity was registered at a scattering angle of 90° at 25 °C. Zeta potentials were measured by a Zeta Plus instrument with Brookhaven electrodes coated by palladium. The zeta potential was the average value of analyses in triplicate.

2.10. Transmission electron microscope (TEM) observations

The morphology of WSC–PASP–PEG nanoparticles was gained by using a Tecnai G2 20S—TWIN transmission electron microscope. A drop of nanoparticle, suspension was mounted on a carbon film coated on a copper grid for viewing. Observation was made at 200 KV in a Tecnai G2 20S—TWIN transmission electron microscope.

2.11. Fourier-transform infrared measurement

The Fourier-transform infrared (FTIR) spectra of the nanoparticulate samples were also identified to determine the interaction between $-NH_3^+$ of WSC and $-COO^-$ of PASP. The WSC–PASP–PEG nanoparticles were lyophilized (Flexi-Dry) to obtain dried particles. The WSC–PASP–PEG nanoparticles so obtained were mixed with KBr and pressed in a pellet for further measurement.

2.12. Swelling test

The dry nanoparticles (100 mg) were immersed in solutions of different pH for 24 h at room temperature until a swollen equilibrium was reached. The swollen samples were collected by filtration, blotted with filter paper for the removal of the absorbed water on the surface, and then weighed immediately. The swelling ratio was calculated using the following equation:[33]

$$\text{Swelling ratio } (\%) = \frac{W_s - W_d}{W_d} \times 100$$

where, W_s and W_d are the weights of swollen and dry samples, respectively.

2.13. Determination of BSA-loading capacity and encapsulation efficiency of the nanoparticles

Bound and unbound BSA were separated by ultracentrifugation of the nanosuspension at 38,000 rpm at 4 °C for 60 min (Optima LE-80k Ultracentrifuge, Beckman).The amount of free BSA in the clear supernatant was measured by a Bradford protein assay using a UV Spectrometer at 595 nm (Shimadzu UV 2550, Japan).[34] The BSA encapsulation efficiency (EE) and loading capacity (LC) of the nanoparticles were calculated using the following equation:

$$\text{EE } \% = \frac{\text{total protein} - \text{free protein}}{\text{total protein}} \times 100\%$$

$$\text{LC } \% = \frac{\text{total protein} - \text{free protein}}{\text{nanoparticles weight}} \times 100\%$$

All measurements were performed in triplicate and averaged.

2.14. In vitro release studies

The in vitro release profiles of BSA from WSC–PASP–PEG nanoparticles were determined as follows: the BSA-loaded WSC–PASP–PEG nanoparticles separated from 9 mL of suspension were placed into test tubes with 6 mL of PBS at pH 7.4 and incubated at 37 °C under stirring at 60 rpm. At appropriate intervals samples were ultracentrifuged, and 1 mL of the supernatant was replaced by fresh medium. The amount of BSA released from the nanoparticles was evaluated by the Bradford method.[34] The calibration curve was made using non-loaded BSA nanoparticles as a correction. All release tests were run in triplicate, and the error bars in the plot show the standard deviation.

2.15. Cell viability

Cell viability was evaluated by using the NIH 3T3 cell line. The cells were cultured in Dulbecco's modified Eagle's medium (DMEM) in a humidified atmosphere (5% CO_2:95% O_2). The cells were seeded into 96-well plates at 10,000 cells per well. The plates were then returned to the incubator, and the cells were allowed to grow to confluence for 24 h. Various nanoparticles were dissolved in DI water. After filtration through a filter paper, the resulting solution was diluted with culture medium to give a final range of concentrations from 0.1 to 1.5 mg/mL. Then the media in the wells were replaced with the pre-prepared culture medium—sample mixture (200 μL). The plates were then returned to the incubator and maintained in 5% CO_2 at 37 °C for 48 h. Each sample was tested in six replicates per plate. After incubation the culture medium and 20 μL of MTT solutions were used to replace the mixture in each well. The plates were then returned to the incubator and incubated for a further 4 h in 5% CO_2 at 37 °C. Then, the culture medium and MTT were removed. DMSO (150 μL) was then added to each well to dissolve the formazan crystals. The plate was placed in 5% CO_2 at 37 °C for 10 min and for 15 min at 6 °C before measurement. The optical density was read on a microplate reader at 490 nm. Cell viability was determined as a percentage of the negative control (untreated cells).

2.16. Circular dichroism (CD) measurements

Circular dichroism (CD) spectroscopy (Jascow 715 spectropolarimeter) was used to measure the conformational change of the released BSA with respect to the native one. Solution of the native BSA or the released BSA was diluted to 0.1 mg/mL and scanned over the wavelength range 200–260 nm, using a 1-mm quartz cylindrical cell.[35]

3. Results and discussion

In this study, a novel nanoparticle system composed of WSC and PASP was prepared with a simple and mild coagulation method under magnetic stirring at room temperature. This technique is promising because the nanoparticles can be prepared under mild conditions without using harmful solvents. It is well known that organic solvents may cause denaturation of peptide or protein drugs that are unstable and sensitive to their environments.[36] The prepared nanoparticles modified by PEG are intended to be used to protect the peptide drugs from denaturalizing in the GI tract and facilitate their transportation into systemic circulation.[37,38]

3.1. The mechanism of the formation of the nanoparticles

In particular, the polyelectrolyte complex is formed by the reaction of two oppositely charged polymers. The electrostatic interaction between the positive charge of $-NH_3^+$ group and the negative charge of carboxyl group is one of the most important factors. The formation and properties of the polymer complex depend on the charge ratio of the anionic-to-cationic species.[39] When PASP is dropped into WSC solution, inter- and intramolecular electrostatic attractions occur between the anionic carboxyl group from PASP and the cationic amino groups of WSC. PEG was incorporated as a third polymer in the system. The carboxyl group in PASP can act as good proton donor, while the ether group of PEG serves as a proton acceptor, thus making interpolymer interactions stronger. These attractions could make the macromolecular chains of WSC and PASP curl up, which leads to the formation of an insoluble WSC–PASP complex.[40,41] A schematic representation of the complex is shown in Figure 2.

Figure 2. Interaction mechanism of WSC–PASP–PEG nanoparticles.

3.2. FTIR spectrum analysis

The interaction of WSC and PASP was first investigated by using FTIR spectroscopy. As seen in Figure 3, for the IR spectrum of WSC, the characteristic peak at 1550 cm^{-1} corresponds to protonated amino groups. In the spectrum of PASP, the characteristic absorption peaks appear at 1597 cm^{-1} and 1403 cm^{-1}. The two strong peaks are observed due to the asymmetrical and symmetrical COO^- groups, respectively. These results indicate that some carboxylic groups of PASP have been dissociated into COO^- groups, which will be able to complex with the protonated amino groups of WSC through electrostatic interactions to form the polyelectrolyte complex. Hence, in the IR spectrum of WSC–PASP nanoparticles, the peaks of COO^- in PASP become weak and shift to 1557 cm^{-1} and 1397 cm^{-1}, respectively.

3.3. Turbidimetric titration measurement and effect of the molar ratio of WSC and PASP on nanoparticles

The formation of colloids based on polyelectrolyte complexes of WSC and PASP nanoparticles was studied as a function of the mixing molar ratio. Four kinds of phenomena were observed in turn during the addition of WSC solution into PASP solution: clear solution, light opalescent, opalescent and precipitation (Table 1). As shown in Figure 4, the absorbance heightened along with the increasing molar ratio of WSC recorded. The absorbance increased sharply when the WSC:PASP (molar ratio) was up to the ratio of 1.43:1. Further increase in molar ratio led to system precipitation, at which point absorbance began to decrease. While the turbidity of WSC–PASP nanoparticles was obtained through the slow addition of PASP solution into WSC solution, it would be out of control.

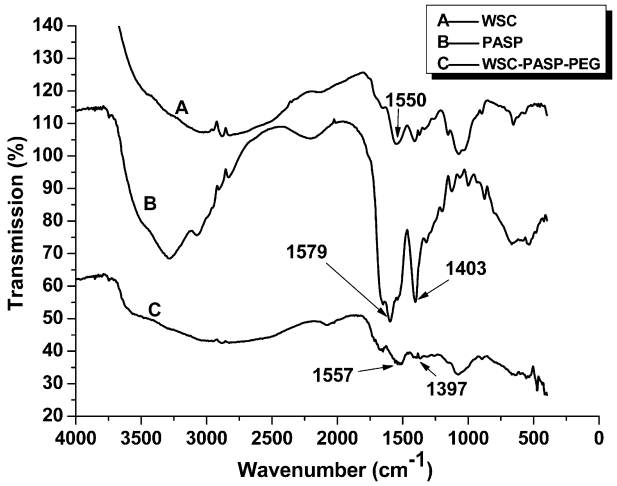

Figure 3. FTIR spectra of the WSC, PASP, and CPP nanoparticles.

Table 1
Effect of the molar ratio of WSC and PASP on the particle sizes of nanoparticles

WSC/PASP (n/n)	Status	Mean size (nm)	Zeta potential (mv)	Process yield (%)
1.78/1	Precipitation	—	—	—
1.43/1	Opalescent	209.0 ± 16.2	+20.21 ± 0.83	45.3 ± 4
1.25/1	Opalescent	182.8 ± 10.5	+19.82 ± 1.25	55.0 ± 3
1.07/1	Light opalescent	137.1 ± 32.2	−33.89 ± 4.33	29.1 ± 3
0.71/1	Light opalescent	99.00 ± 23.7	−20.38 ± 3.67	1.20 ± 5
0.36/1	Clear solution	—	—	—

It is probably due to the difference of M_r. Because M_r of PASP is much larger than that of WSC, the charge molar ratio was also large. It led to the turbidity increase sharply. This proved the formation of insoluble polyelectrolyte complexes since neither WSC nor PASP absorbed light at 500 nm.

It was found that only when the molar ratio of WSC to PASP was lower than 1.43:1, the nanoparticles could be formed. The nanoparticles thus prepared carried a positive or negative charge and had a mean size in the range of 100–200 nm. From the zeta potential data, when the CS:DS molar ratio increased, the zeta potential varied from a negative charge to a positive charge. The magnitude of the zeta potential gives an indication of the potential stability of the nanoparticle system. All the nanoparticles have negative or positive charge, they will repel each other, and there is dispersion stability. This system can be stable for more than two weeks without aggregation.

In Figure 5, the result showed that the colloidal dispersions were stable due to the electrostatic repulsion, which prevented further coagulation. Figure 6 shows the morphological characteristics of the nanoparticles. CPP nanoparticles modified by PEG were spherical in shape and about 160 nm in diameter. The chosen molar ratio was equal to 1.25:1 as the research sample for other characterizations.

3.4. Effect of polyethylene glycol concentration on nanoparticles

From Figure 7, with the concentration of PEG increasing, the size of the nanoparticles decreased. The incorporation of PEG and WSC–PASP nanoparticles was through intermolecular hydrogen between the electropositive amino hydrogen of WSC and the electronegative oxygen atom of PEG. Thus WSC–PEG–PASP semi-interpenetration network was formed. Additionally, PASP can form interpolymer complexes with PEG through cooperative hydrogen

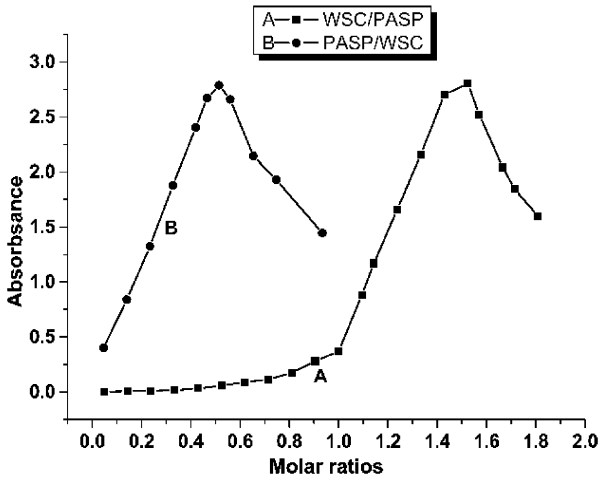

Figure 4. (A) The turbidity titration of WSC–PASP nanoparticles obtained by slow addition of a WSC solution into a PASP solution; (B) the turbidity titration of WSC–PASP nanoparticles obtained by slow addition of a PASP solution into a WSC solution.

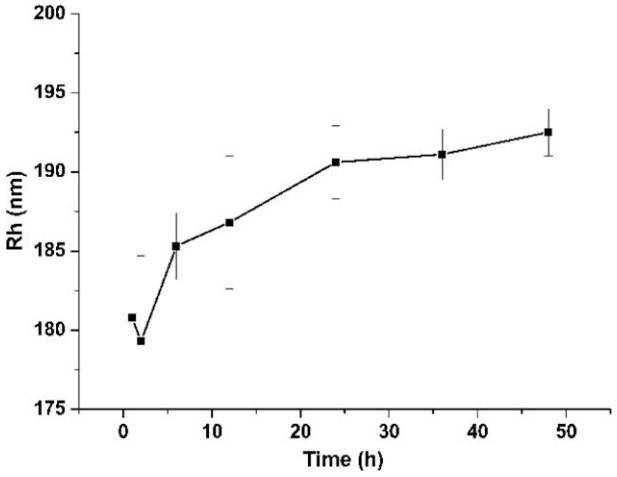

Figure 5. Evaluation of nanoparticles size at different time (Rh is the fluid dynamic radius).

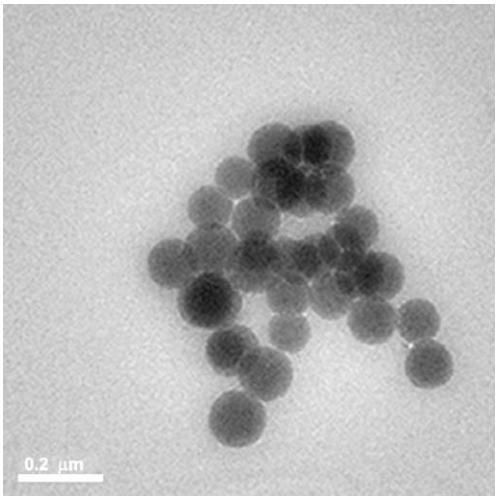

Figure 6. TEM of CPP nanoparticles.

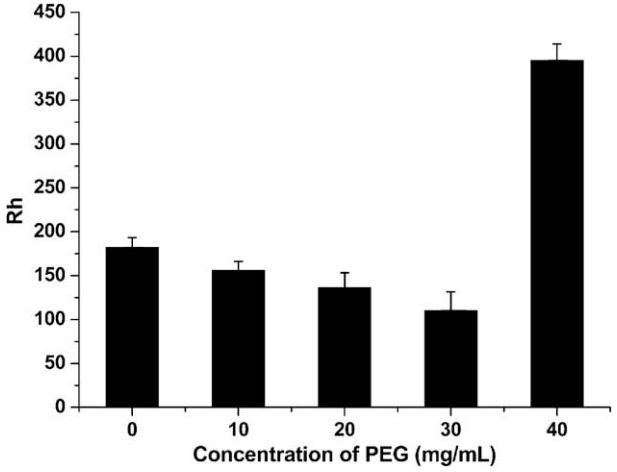

Figure 7. Effect of PEG concentration on the size of nanoparticles.

bonding amongst acid-ether groups. Carboxyl groups in PASP can act as proton donors, thus making interpolymer interactions stronger. When the concentration of PEG was up to 40 mg/mL, the mean size increased sharply. This may be because there were so many hydrogen bonds that two or more nanoparticles congregated.

3.5. Effect of ionic strength on nanoparticles

The effect of ionic strength on the size of nanoparticles is shown in Figure 8. The size of the nanoparticles increases along with the addition of NaCl solution with the concentration in the range of 0.005–0.025 mol/L. When C_{NaCl} >0.025 M, the size of the nanoparticles decreases along with the addition of NaCl solution. The observed phenomenon probably results from two competing effects. On one hand, the addition of salt favors the formation and the growth of nanoparticles, which is indicated by the increase in the number and size of nanoparticle aggregates.[42] On the other hand, the addition of salt interferes with the electrostatic attraction between the polymer chains of opposite charge, which reduces the interaction. Therefore, at low salt concentrations, the effect on the formation and growth of nanoparticles may exceed the screening of the interaction, which leads to the enhancement of the final interaction. At higher salt concentrations, the dominant screening of the interaction leads to the total reduction of the interaction.

3.6. Effect of pH on nanoparticle swelling behavior

In order to investigate the effect of pH values on CPP nanoparticles, a series of experiments were carried out. As shown in Figure 9, the swelling ratio of various samples is plotted as a function of pH. It is known that the pK_a values of PASP and WSC are 4.4 and 6.5, respectively.[43] At pH 1.2, the increased swelling may be caused by the dissociation of ionic bonds between WSC and PASP. As most of the carboxyl acid groups are protonated, and amino groups are in the $-NH_3^+$ form, so the molecules have net positive charge. It is probably because the water-soluble chitosan assumes a randomly extended conformation in the low pH region, due to both hydration of the protonated amino group and a strong positive charge repulsion among the $-NH_3^+$ groups, which will lead to the swelling of the WSC–PASP nanoparticles. At a pH near to 5.0, the amino groups in WSC are protonated and the carboxyl groups in a PASP are ionized; thus, the strong electrostatic attractions between WSC and PASP restrain the swelling of nanoparticles. At high pH, most of the amine groups of WSC are in the $-NH_2$ form, and most of the carboxyl groups of PASP are in the $-COO^-$ form, and so the electrostatic attractions were weakened in nanoparticles, thus increasing nanoparticle swelling. The nanoparticles show pH sensitivity, a property that can be used for the development of drug delivery systems.

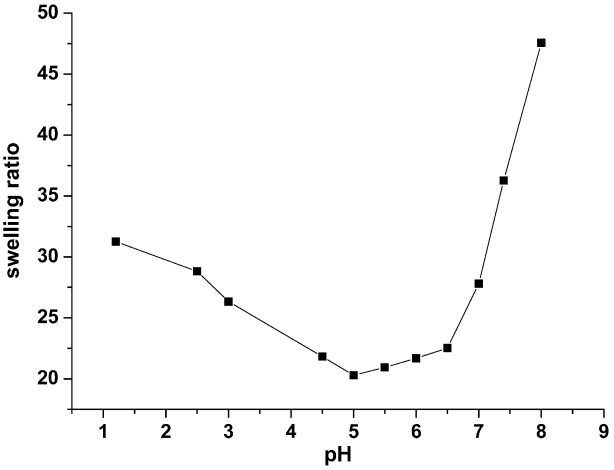

Figure 9. Effect of pH on the swelling ratio.

3.7. BSA encapsulation efficiency of the nanoparticles and release behavior in vitro

BSA encapsulation efficiency and loading capacity of CPP nanoparticles were studied under six different concentrations of BSA (0.5, 1.0, 1.5, 2.0, 2.5 and 3.0 mg/mL). Encapsulation efficiency and loading capacity of nanoparticles are shown in Figure 10, which clearly indicates that encapsulation efficiency of these particles was affected by initial concentration of the protein used. As the initial concentration of BSA was increasing, encapsulation efficiency decreased slowly while loading capacity increased. An approximate 90% encapsulation efficiency was observed for these particles when the initial concentration of BSA was 0.5 mg/mL. As the initial concentration of BSA increased up to 3.0 mg/mL, the encapsulation efficiency decreased by less than 60%, while loading capacity increased by more than 40%.

The release of BSA from CPP nanoparticles was performed in the buffer solution of pH 1.2, 2.5 and 7.4, respectively, which was simulation of the condition of pH in the GI tract. Figure 11 depicts the release profiles of BSA at pH 1.2, 2.5 and 7.4. Particles with carbox-

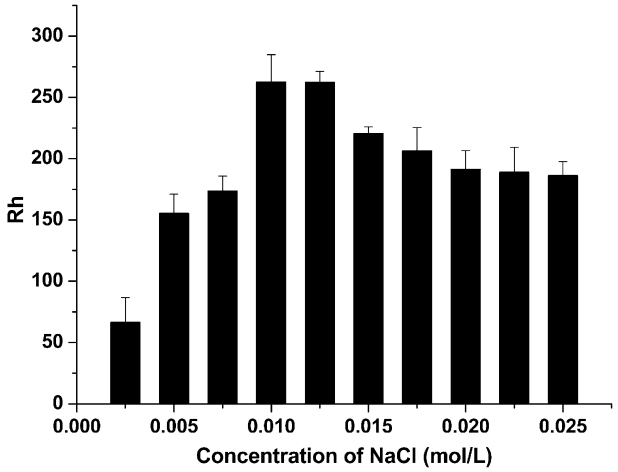

Figure 8. Effect of salt concentration on the size of nanoparticles.

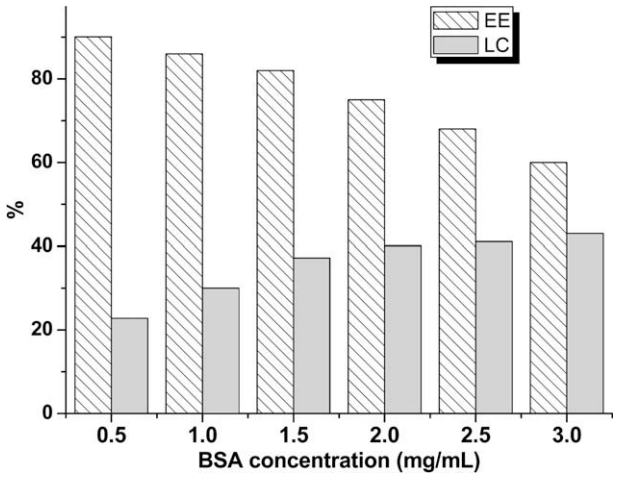

Figure 10. BSA encapsulation efficiency and loaded capacity of CPP nanoparticles.

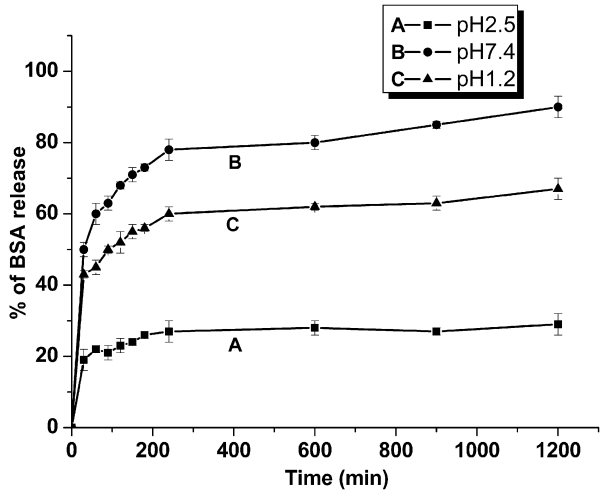

Figure 11. In vitro release of BSA from CPP nanoparticles at different pH values.

ylic acid groups swell in weakly alkaline or neutral pH, and protein diffuses into the matrix quite easily. In other words, particles containing carboxylic acid groups display pH-sensitive, swelling/deswelling behavior with the protonation/deprotonation of the carboxylic acid groups. At pH 1.2 (simulating the pH in the stomach after a meal), most carboxylic groups of PASP were in the form of COOH, and there was little electrostatic interaction between WSC and PASP. In addition, the particles became unstable and subsequently broke apart. At pH 2.5 (simulating the pH environments of a fasting stomach), the amount of BSA released from the nanoparticles was about 20% within the first 2 h. Therefore, the nanoparticles prepared in the study may be orally administered only before meals (pH 2.5–3.7). Similarly, at pH 7.4 (simulating the pH oft the bloodstream), in the first 2 h, more than 60% of the BSA was released. WSC was deprotonated, which led to the collapse of the nanoparticles. Finally, it is noted that the nanoparticles present a pH-dependent release pattern, which can not only protect protein drug loss in an acid environment but also control drug release in the GI tract.

3.8. Cell viability

Cell viability was used to evaluate the biocompatibility of the nanoparticles. In order to further evaluate the role of WSC, the chitosan (CS) with high molecular weight was evaluated. The cells were exposed to CPP, CS–PEG–PASP nanoparticles, and the nanoparticulate dispersions at various concentrations were incubated for 48 h (Fig. 12). As shown in Figure 12, the CPP nanoparticle system has a better biocompatibility than the other one. The CS–PEG–PASP has lower cell viability than CPP nanoparticles. This may be due to chitosan which has a high molecular weight and needs to be dissolved in an HOAc solution at a pH value of approximately 4.0. One possible explanation for this can be ascribed to the cell toxicity of the acid solution. Under these circumstances, the bioactivity of the cells are easily damaged. The CPP nanoparticles also have better biocompatibility than WSC–PASP. PEG is probably one of the best-known hydrophilic polymers, and incorporation of PEG can increase biocompatibility. The results suggest that CPP nanoparticles may be good biocompatible carriers for drug delivery and may have potential for in vivo use.

3.9. Circular dichroism (CD) spectra

Circular dichroism spectroscopy has been used to examine the conformation and self-association of BSA. There are three common secondary structures in BSA, namely α helices, β sheets, and turns. The native BSA has two extreme valleys at 208 and 222 nm.[44] Since α helices are one of the elements of secondary structure, the quantitative analysis of the structural change of BSA can be evaluated by determining the amount of α helix preserved. The α helix content of a protein is estimated according to the following equation:[35]

$$\%\ \alpha\text{-helix content} = \frac{\theta_{mrd} - 4000}{33000 - 4000}$$

where, θ_{mrd} is the mean molar ellipticity per residue at 208 nm (deg cm^2 dmol^{-1}). Usually the raw data from the experiment are expressed in terms of θ_d (the ellipticity in the unit of mdeg). However, it can be converted to mean molar ellipticity per residue using the following equation:[45]

$$\theta_{mrd} = \frac{\theta_d M}{10CLN}$$

where, M is the BSA molecular weight (Da), C is the BSA concentration (mg/mL), L is the sample cell path length (cm), and N is the number of amino residues. As indicated by the CD spectra (Fig. 13), the native BSA has 50% α helix, which is close to the literature value of 48%.[46] After release from CPP nanoparticles, the α helix content is 47%, which is very close to that of the native BSA. In other words, no significant conformational change was noted

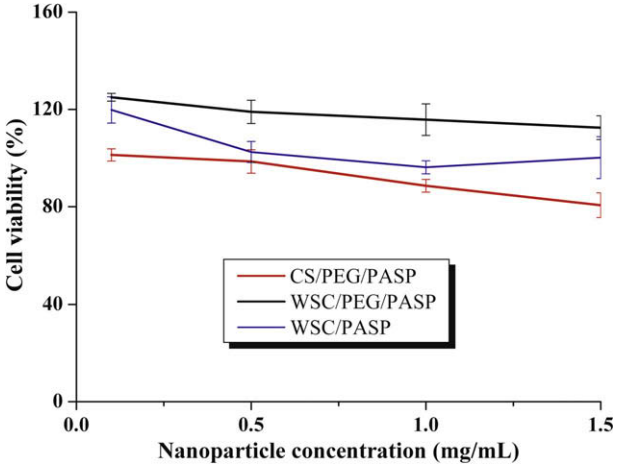

Figure 12. Viability of cells after incubation as a function of nanoparticle concentration by MTT assay, at 37 °C for 48 h.

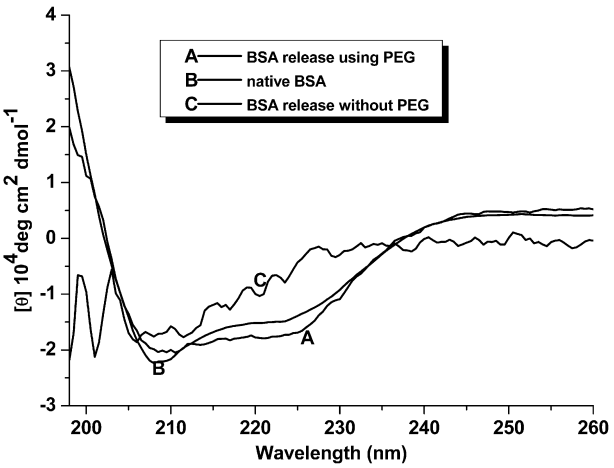

Figure 13. Circular dichroism (CD) spectra of BSA released from test nanoparticles at pH 7.4 and native BSA.

for the BSA released from the CPP nanoparticles at pH 7.4 as compared with the native BSA. However, the BSA that was released from the nanoparticles without PEG has obviously changed its conformation. On the one hand, microencapsulation of protein drugs onto hydrophobic matrices involves use of either organic solvents and/or high temperature, and these conditions may reduce their biological activities. Without using harmful solvents, which may cause degradation of peptide or protein drugs that are unstable and sensitive to their environments, the protein drugs have not been distorted. On the other hand, segmental flexibility and uncharged chemical composition of PEG help to readily adapt their conformations to fit the surface topology of proteins.[25] Therefore, polyethylene glycol was chosen as a protein-protective agent.

4. Conclusions

Polyelectrolyte complexation among WSC, PEG and PASP was investigated through the formation of a nanoparticulate system driven by electrostatic interactions. This study showed that WSC–PASP–PEG nanoparticles can be spontaneously formed through combinations of opposing ions under mild conditions without the need of organic solvents, surfactants, or special experimental technologies. Physicochemical properties of the particles, such as mean size, zeta potential, and process yield, were dependent on the molar ratio of WSC:PASP. FTIR analyses of the nanoparticles demonstrated evidence of polyelectrolyte complex formation. Factors such as WSC:PASP molar ratios, concentration of PEG, pH and ionic strength of the release medium, have a huge effect on the results in this study. The encapsulation efficiency of BSA-loaded WSC–PASP–PEG nanoparticles varied from 60% to 90% depending on the initial loading concentration of BSA. The in vitro drug release characteristics of WSC–PASP–PEG nanoparticles were also investigated, and it was shown that these nanoparticles were able to sustain the release of BSA under simulated colonic conditions. These nanoparticles that undergo complex formation have demonstrated potential as carriers for the oral delivery peptide or protein drugs.

References

1. Takakura, Y.; Kaneko, Y.; Fujita, T.; Hashita, M.; Maeda, H.; Sezaki, H. *J. Pharm. Sci.* **1989**, *78*, 117–121.
2. Castro, G. R.; Kamdar, R. R.; Panilaitis, B.; Kaplan, D. L. *J. Controlled Release* **2005**, *109*, 149–157.
3. Ponchel, G.; Irache, J. M. *Adv. Drug Delivery Rev.* **1998**, *34*, 191–219.
4. Russell-Jones, G. J. *J. Controlled Release* **2000**, *65*, 49–54.
5. Sood, A.; Panchagnula, R. *Chem. Rev.* **2001**, *11*, 3275–3304.
6. Hu, Y.; Jiang, X. Q.; Ding, Y.; Ge, H. X.; Yuan, Y. Y.; Yang, C. Z. *Biomaterials* **2002**, *23*, 3193–3201.
7. Aboubakar, M.; Couvreur, P.; Pinto-Alphandary, H.; Gouritin, B.; Lacour, B.; Farinotti, R.; Puisieux, F.; Vauthier, C. *Drug Dev. Res.* **2000**, *49*, 109–117.
8. Gref, R.; Minamitake, Y.; Peracchia, M. T.; Trubetskoy, V.; Torchilin, V.; Langer, R. *Science* **1994**, *263*, 1600–1603.
9. Guzman, M.; Aberturas, M. R.; Rodriguez-Puyol, M.; Molpeceres, J. *Drug Deliv.* **2000**, *7*, 215–222.
10. Wehrle, P.; Magenheim, B.; Benita, S. *Eur. J. Pharm. Biopharm.* **1995**, *41*, 19–26.
11. Tsuchida, E.; Abe, K. *Adv. Polym. Sci.* **1982**, *45*, 1–119.
12. Lee, S. B.; Lee, Y. M.; Song, K. W.; Park, M. H. *J. Appl. Polym. Sci.* **2003**, *90*, 925–932.
13. Feng, Q.; Zeng, G.; Yang, P.; Wang, C.; Cai, J. *J. Colloids Surf., A* **2005**, *85*, 257–258.
14. Kim, S. J.; Shin, S. R.; Lee, K. B.; Park, Y. D.; Kim, S. I. *J. Appl. Polym. Sci.* **2004**, *91*, 2908–2913.
15. Arguelles-Monal, W.; Cabrera, G.; Peniche, C.; Rinaudo, M. *Polymer* **2000**, *41*, 2373–2378.
16. Tapia, C.; Escobar, Z.; Costa, E.; Sapag-Hagar, J.; Valenzuela, F.; Basualto, C.; Nella-Gai, M.; Yazdani-Pedram, M. *Eur. J. Pharm. Biopharm.* **2004**, *57*, 65–75.
17. Yin, Y. J.; Yao, K. D.; Cheng, G. X.; Ma, J. B. *Polym. Int.* **1999**, *48*, 429–432.
18. Schatz, C.; Domard, A.; Viton, C.; Pichot, C.; Delair, T. *Biomacromolecules* **2004**, *5*, 1882–1892.
19. Nge, T. T.; Yamaguchi, M.; Hori, N.; Takemura, A.; Ono, H. *J. Appl. Polym. Sci.* **2002**, *83*, 1025–1035.
20. Barck, K.; Butler, M. F. *J. Appl. Polym. Sci.* **2005**, *98*, 1581–1593.
21. Lavertu, M.; Xia, Z.; Serreqi, A. N.; Berrada, M.; Rodrigues, A.; Wang, D.; Buschmann, M. D.; Gupta, A. J. *J. Pharm. Biomed.* **2003**, *32*, 1149–1158.
22. Ashmore, M.; Hearn, J.; Karpowicz, F. *Langmuir* **2001**, *17*, 1069–1073.
23. Smith, J.; Wood, E.; Dornish, M. *Pharm. Res.* **2004**, *21*, 43–49.
24. Schipper, N. G. M.; Olsson, S.; Hoogstraate, J. A.; Deboer, A. G.; Vårum, K. M.; Artursson, P. *Pharm. Res.* **1997**, *14*, 923–929.
25. Harris, J. M. *Poly(Ethylene Glycol) Chemistry: Biotechnical and Biomedical Applications*; Plenum Press: New York, 1992; pp 1–12.
26. Doillon, C. J.; Cote, M. F.; Pietrucha, K.; Laroche, G.; Gaudreault, R. C. *J. Biomater. Sci., Polym. Ed.* **1994**, *6*, 715–728.
27. Roberts, M. J.; Bentley, M. D.; Harris, J. M. *Adv. Drug Delivery Rev.* **2002**, *54*, 459–476.
28. Peppas, N. A.; Keys, K. B.; Torres-Lugo, M.; Lowman, A. M. *J. Controlled Release* **1999**, *62*, 81–87.
29. Zheng, Y. L.; Yang, W. L.; Wang, C. C.; Hu, J. H.; Fu, S. K.; Dong, L.; Wu, L. L.; Shen, X. Z. *Eur. J. Pharm. Biopharm.* **2007**, *67*, 621–631.
30. Masayuki, T.; Takeshi, N.; Mayumi, K.; Minako, S.; Shigeyuki, M.; Toyoji, K. *Polymer* **1996**, *37*, 4435–4437.
31. Masayuki, T.; Takeshi, N.; Shigeyuki, M.; Toyoji, K. *Polymer* **1997**, *38*, 4733–4736.
32. Alonso-Sande, M.; Cuna, M.; Remunan-lopez, C.; Teijeiro-Osorio, D.; Alonso-Lebrero, J. L.; Alonso, M. J. *Macromolecules* **2006**, *39*, 4152–4158.
33. Dai, Z. Z.; Yin, J. B.; Yan, S. F.; Cao, T.; Ma, J.; Chen, X. S. *Polym. Int.* **2007**, *56*, 1122–1127.
34. Bradford, M. M. *Anal. Biochem.* **1976**, *72*, 248–254.
35. Greenfield, N.; Fasman, G. D. *Biochemistry* **1969**, *8*, 4108–4116.
36. Kajihara, M.; Sugie, T.; Hojo, T.; Maeda, H.; Sano, A.; Fujioka, K.; Sugawara, S.; Urabe, Y. *J. Controlled Release* **2001**, *73*, 279–291.
37. Vila, A.; Sanchez, A.; Evora, C.; Soriano, I.; McCallion, O.; Alonso, M. J. *Int. J. Pharm.* **2005**, *292*, 43–52.
38. Hans, M. L.; Lowman, A. M. *Curr. Opin. Solid State Mater.* **2002**, *6*, 319–327.
39. Baier, J.; Koetz, J.; Kosmella, S.; Tiersch, B.; Rehage, H. *J. Phys. Chem. B* **2007**, *111*, 8612–8618.
40. Chluba, J.; Voegel, J. C.; Decher, G.; Erbacher, P.; Schaaf, P.; Ogier, J. *Biomacromolecules* **2001**, *2*, 800–805.
41. *Handbook of Polyelectrolytes and Their Applications*; Nalva, H. S., Ed.; American Scientific Publishers: New York, 2002.
42. Schneider, G.; Decher, G. *Langmuir* **2008**, *24*, 1778–1789.
43. Wu, Y. T.; Grant, C. *Langmuir* **2002**, *18*, 6813–6820.
44. Peng, Z. G.; Hidajat, K.; Uddin, M. S. *Colloids Surf., B* **2004**, *33*, 15–21.
45. Xu, Y. M.; Du, Y. M.; Huang, R. H.; Gao, L. P. *Biomaterials* **2003**, *24*, 5015–5022.
46. Bouillot, P.; Ubrich, N.; Sommer, F.; Duc, T. M.; Loeffler, J. P.; Dellacherie, E. *Int. J. Pharm.* **1999**, *181*, 159–172.